Mon. Not. R. Astron. Soc. **384,** 1588–1596 (2008) doi:10.1111/j.1365-2966.2007.12827.x

HR 710 (HD 15144): an ultra-Sr-rich, magnetic Ap star with a close companion⋆

C. R. Cowley[1]† and S. Hubrig[2]†

[1]*Department of Astronomy, University of Michigan, Ann Arbor, MI 48109-1042, USA*
[2]*European Southern Observatory, Casilla 19001, Santiago 19, Chile*

Accepted 2007 December 5. Received 2007 December 4; in original form 2007 October 14

ABSTRACT

The magnetic, chemically peculiar A-star HR 710 (HD 15144, ADS 1849A, AB Cet) has a close companion in a nearly circular orbit. Its 3-d period is unusually short for such stars. The system emits moderately hard X-rays, which likely come from a white dwarf secondary (ADS 1849Ab). The Sr II spectrum is very strong, and the resonance lines show similar core-nib structure to the stronger Ca K line. We place only loose constraints on a model. There are indications of a lower electron/gas pressure than expected from the star's parallax and brightness. Strong-line profiles and anomalous excitation/ionization indicate significant deviations from traditional models, fixed by $T_{\rm eff}$, $\log g$ and abundances. Weak spectral-line profiles and wavelength shifts probably indicate abundance patches rather than the presence of a secondary (ADS 1849Ab) spectrum. Our UV–Visual Echelle Spectrograph (UVES) spectra are from only one epoch. Additional low-noise, high-resolution spectra are needed. We discuss the spectrum within the context of abundance stratification.

Key words: stars: atmospheres – stars: chemically peculiar – stars: individual: HR710 – stars: magnetic fields.

1 INTRODUCTION

Roman (1949) listed HR 710 (HD 15144) among the probable members of the Ursa Major Stream. She noted the strengths of λλ4077 and 4215. More recently, King et al. (2003) enter a question mark in the column for 'Final Memb.' for HD 15144A. Tokovinin (1997) concludes that the system ADS 1849AB is a physical double, rather than a common proper motion pair, but the period must be very long. The primary, ADS 1849A (or is itself a spectroscopic binary (Aa and Ab) with a well-determined period of 2.998 d (Bonsack 1981; Tokovinin 1997). This is a very short period for a magnetic Ap star. One system, HD 200405 (cf. Carrier et al. 2002), with an even shorter period is known −1.64 d. The HR 710 system appears to be single lined, so there has been a large uncertainty in the mass and luminosity of the companion.

Hünsch, Schmitt & Voges (1998) list HR 710 in their *ROSAT* survey of main-sequence and subgiant stars of the Bright Star Catalogue. They found an X-ray luminosity of 4.2×10^{29} erg s^{-1}. This is among the top third of the group. The hardness ratio they report, 0.12, is in the upper 15 per cent. Thus HR 710 is significant, though not outstanding among these X-ray emitters.

Czesla & Schmitt (2007) report *Chandra* observations of HR 710 as well as the companion ADS 1849B in the energy band 0.5–2 keV. Their X-ray flux for the primary is in reasonable agreement with the *ROSAT* data.

Extensive magnetic field measurements were made by Babcock (1958) and Bonsack (1981). The field varied between −0.45 and −1.10 kG – it did not reverse. Bonsack's plot of $H_{\rm eff}$ folded on the 3-d orbital period appears random. These results are consistent with nearly magnetic and rotational pole-on observations. Bonsack sought other periods, and found marginal evidence for a 15.88-d period. He concluded $\langle H_{\rm eff}\rangle \approx -700$ G, with an rms error of a single observation of 140 G.

One of us, CRC, measured wavelengths of a 2.4 Å mm^{-1} spectrum from the Dominion Astrophysical Observatory in 1979. Contemporary notes include a remarks on the strengths of Sr II and Ca II K. Additionally, they note the subordinate Sr II line, 4305.45, 'has huge wings' (see Fig. 1). Our description is similar to that of Babcock (1958), who also pointed out that *lines of Sr II, like the K line, have strong, sharp cores with wide shallow wings*. Much of the present study follows this lead.

Otherwise, the spectrum was not found unusual among the variegated spectra of CP types. Iron-group spectra, including Sc II (but not V II), are rich, while Y II and Zr II are not as strong as one might expect given the outstanding strength of Sr II. The lanthanides are present, but not remarkable in richness or in strength. The strong Eu II lines at λλ4129 and 4205, for example, are exceeded in strength by nearby lines of iron-peak elements.

⋆Based on observations obtained at the European Southern Observatory, Paranal and La Silla, Chile [ESO programmes 076.D-0169(A) and 076.C-0172(A)].

†E-mail: cowley@umich.edu (CRC); shubrig@eso.org (SH)

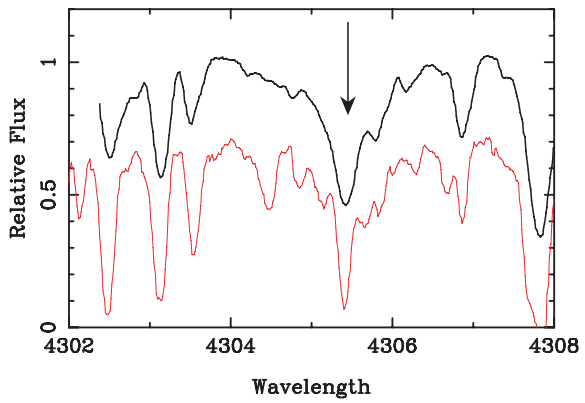

Figure 1. The subordinate line Sr II at 4305.47 Å. The transition is $5p^2P^0_{3/2}$–$6s^2S_{1/2}$. The lower excitation potential is 3.04 eV. The upper spectrum is of HR 710, while the lower is of γ Equ. The latter spectrum is displaced downward by 0.3 for display purposes. Although both stars are classified as strontium stars, the wings on λ4305 are arguably more pronounced in HR 710 than in the sharper lined spectrum of γ Equ.

We know of no modern abundance study of HR 710. It was among several Ap stars analysed in the 1960s, with rather crude methods by today's standards, and only selected elements were studied. For example, the work of Searle, Lungershausen & Sargent (1966) was restricted to Ti, Mn, Cr and Fe. We would agree with these authors that these particular elements are all enhanced by similar factors.

HR 710 was among the stars studied by Cowley et al. (2007, hereafter CHCGW) for the calcium isotopic anomaly discovered by Castelli & Hubrig (2004). In the course of this work we confirmed that conventional models failed to account for the profiles of the strong Ca II lines. This was in complete agreement with results of Ryabchikova and her coworkers [see e.g. Ryabchikova et al. (2002, fig. 3)]. These workers have used a stratified-abundance model to fit Ca I and Ca II and other metallic lines, as described in subsequent studies on numerous magnetic Ap stars (cf. Ryabchikova, Kochukhov & Bagnulo 2007).

For γ Equ, we found that essentially the same model fit the λ8542 line of the infrared triplet (henceforth, IRT, cf. fig. 7 of CHCGW). The same stratification provided a reasonably good fit to the λ8498 line.

In the course of research leading to CHCGW a number of lines were synthesized that were not discussed in that work. Provisional calculations for HR 710 showed we would have difficulty matching the profiles of the IRT with the same stratification that fit the Ca II K line.

The unusual strength of Sr II in HR 710 deserves closer study. Would a stratified model be required to match the profiles of the Sr II resonance lines λλ4077 and 4215, or the strong subordinate lines? If so, would the study of these features add to our understanding of the structure of the photospheres of magnetic stars? The sections below deal with these questions.

We can place only loose constraints on the physical conditions in the atmosphere of HR 710. In addition to line core/wing and ionization and excitation anomalies, there is evidence for abundance patches on the surface, which can be seen in some of the line profiles.

2 OBSERVATIONS

The ESO spectra used in this study were obtained on 2005 September 19 with the UV–Visual Echelle Spectrograph (UVES) at UT2 of the VLT. The spectra used the new (2004 November) standard Dichroic settings were described by CHCGW, covering 3290–9460 Å. This configuration makes it possible to measure the λ8542 line, which had previously been unavailable because of an order gap. The resolving power is 80 000 in the blue–violet, and 110 000 in the red. The signal-to-noise ratios of the spectra differ, but range from about 100–400.

3 REDUCTIONS

The UVES spectra were reduced by the UVES pipeline Data Reduction Software (version 2.5), which is an evolved version of the echelle context of MIDAS. The spectra were mildly Fourier filtered before the wavelengths were measured at Michigan.

We choose the continuum by picking high points of the relative flux using console displays 40 Å wide. In some cases, a Paschen line or water–vapour band would take up most of the display, and no continuum point would be chosen. The high points were connected by a spline *and* by linear interpolation. After some experimentation the linear fit was given weight 2, the spline 1, and the weighted average adopted. The continuum height is surely uncertain to a few per cent. Nevertheless we note that in the illustrations that follow, no additional (ad hoc) adjustments were made to the continua.

Wavelength measurements from 4527 to 4652 Å are from 2.4 Å mm^{-1} spectra (12766U and V) obtained at the Dominion Astrophysical Observatory in 1979. The instrument has been described by Fletcher, Harmer & Harmer (1980).

4 THE ATMOSPHERE OF HR 710

4.1 Preliminary remarks

Ap stars were once thought to have abnormal abundances, but normal atmospheres. We now know that this is not the case. The profiles of the low Balmer and the strong metallic lines cannot be reproduced by standard plane-parallel atmospheres. Simple adjustments to temperature, gravity and composition do not allow one to resolve inconsistencies in ionization and excitation. These difficulties have become apparent relatively recently. Horizontal chemical inhomogeneities (abundance patches) have been known in magnetic stars for many decades.

Extensive observations by Babcock (1958) and Bonsack (1981) show that spectral variations in HR 710 are mild or absent. Nevertheless, abundance patches apparently influence the spectrum. We acknowledge this, among other complications, but do not treat it in the present study.

4.2 Photometry

We used several codes based on Strömgren or Geneva photometry to try to fix $T_{\rm eff}$ and $\log g$. In addition, we considered ionization balance, Balmer and Paschen profiles. The various implementations give a fairly wide range of values for $T_{\rm eff}$ (8400–8600 K) and $\log g$ (3.0–4.0).

An implementation of Geneva photometry by Kaiser (2006), based on Künzli et al. (1997), includes an adjustment for [Fe/H]. The code gives values of $\log g$ that decrease with increasing [Fe/H]. Allowed entries for [Fe/H] are −1, 0 and +1. The relation for both $\log g$ and $T_{\rm eff}$ is very nearly linear. We used photometric measurements for HR 710 from the Simbad data base to obtain second-order

fits, with very small quadratic terms. With [Fe/H] = +1.0, we obtain $T_{\rm eff} = 8460$ K and $\log g = 3.6$. This somewhat low gravity is supported by our ionization balance of neutral and singly ionized Fe, where we get best agreement with $\log g = 3.0$. This ionization balance (see below) gives a temperature nearly 200 K higher.

Codes based on Strömgren photometry give significantly higher gravities, though they do not, to our knowledge, include a provision to allow for metallicity.

The higher surface gravities agree with the results of Hubrig, North & Schöller (2007), who give $\log g = 4.2$. The temperature estimate from this study is 8433 K.

4.3 Balmer lines

Hydrogen line strengths depend sensitively on temperature in cooler stars, and on surface gravity in hotter ones. HR 710 is at the high-temperature end of the region where the line strengths change from primarily temperature to primarily gravity sensitivity.

All Balmer calculations are based on the profiles from Stehlé & Hutcheon (1999).

Fig. 2 shows the observed and calculated profile of Hα for models with $T_{\rm eff} = 8600$ K, and $\log g = 3.0$ and 4.0. The fit is arguably better with the lower gravity model (upper smooth curve). Metallic lines have been omitted from the calculation to avoid confusion. The tendency of the lower Balmer cores of cooler magnetic Ap stars to be deeper, and sharper than the observations was called the core-wing anomaly (Cowley et al. 2001). Local thermodynamic equilibrium (LTE) calculations of the Hα core are never as deep as the observations. In the case of HR 710, departures of the calculations from the observed profiles in the regions outside the inner core are of interest. For Hα and especially for Hγ and Hδ the calculations do not fit the observations until the far wings are reached.

The case for the lower gravity is somewhat stronger with Hγ (Fig. 3) and Hδ (not shown).

Fig. 4 shows the region of the Balmer confluence. H18 (3691.56) is surely present, and H19 (3686.83) possibly so, though the feature is clearly strengthened by blending primarily with Cr II 3687.03 and Fe I-75 3687.10. The multiplet number (75) is from Moore (1945). The strong Cr II line does not appear in the multiplet tables. The Inglis–Teller relation (cf. Cowley 1970, equation AI-5) yields $\log N_{\rm e} = 13.4$ if the last Balmer line is H19. This electron density is reached in our models with $T_{\rm eff} = 8600$ K, and with $\log g = 4$ at a logarithmic optical depth $\log \tau_{3640} = -0.7$. For the $\log g = 3$ model the corresponding optical depth is -0.08.

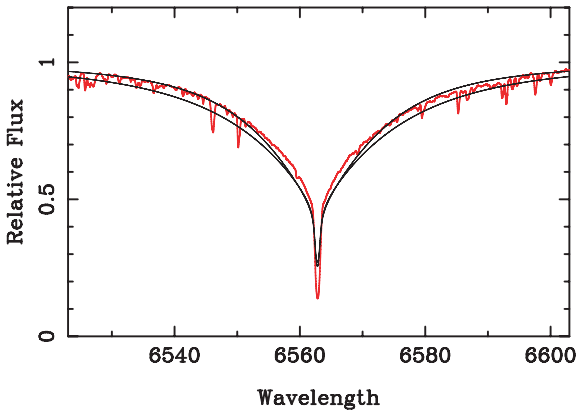

Figure 2. Hα profile in HR 710. The calculated profiles from models with $\log g = 3.0$ (upper curve) and 4.0 (lower curve). In both cases, the assumed temperature is 8600 K.

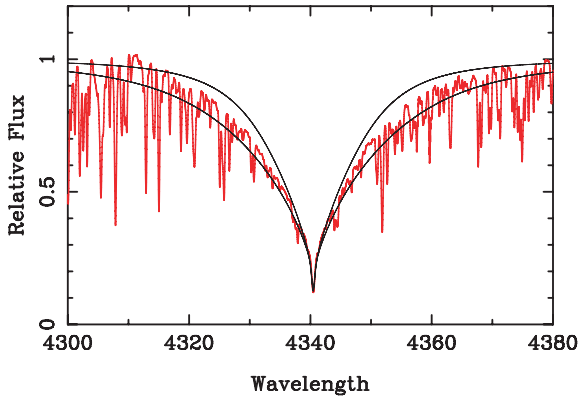

Figure 3. Hγ profile in HR 710. The calculated profiles from models with $\log g = 3.0$ (upper curve) and 4.0 (lower curve). In both cases, the assumed temperature is 8600 K.

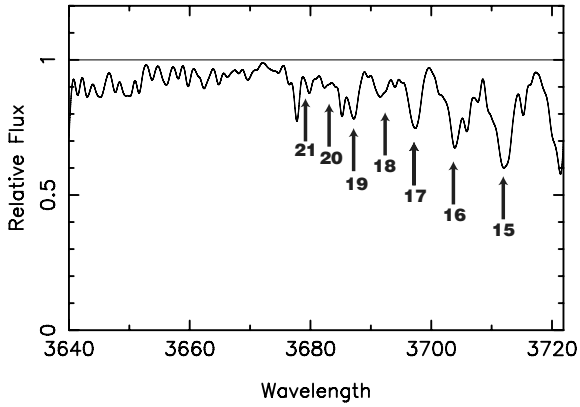

Figure 4. Region of the Balmer confluence. The spectrum has been rather severely filtered in an attempt to make the Balmer lines stand out.

We have used the optical depth at λ3640, short of the Balmer jump. This should closely approximate the opacity where the confluence occurs, *including* the opacity due to overlapping higher Balmer lines. The basis of this statement may be found, among other places, in Cowley (2000, see also Appendix A).

We expect the electron density obtained by the Inglis–Teller formula would correspond to $N_{\rm e}$ at optical depth unity for the wavelength of the Balmer jump. Thus, the last countable Balmer line appears to give mild support for a lower $\log g$ model. However, a plot similar to Fig. 4 for γ Equ shows Balmer components possibly as high as H20. Moreover, in two other main-sequence stars, ν Cap (B9.5 V) and σ Boo (F2 V), we can count to H22 or H23 and H19 or H20, respectively. A detailed study of the usefulness of the last countable Balmer line as an indicator of surface gravity would be worth while.

4.4 Paschen lines

The lower Paschen members are beyond our wavelength coverage. The first usable line is λ9229, P9. The lowest Paschen members, P9, P10 and P11, are clearly fit better with a $\log g = 4$ model than $\log g = 3$. All Paschen line calculations used Lemke's (1997) revised VCS profiles (Vidal, Cooper & Smith 1973), because the

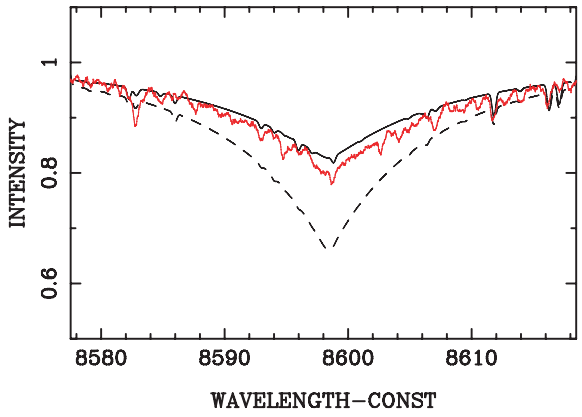

Figure 5. The Paschen line P14. The smooth, solid curve was calculated using a model with $T_{\rm eff} = 8600$ and $\log g = 4$. The dashed line shows the profile from the lower gravity model, $\log g = 3$.

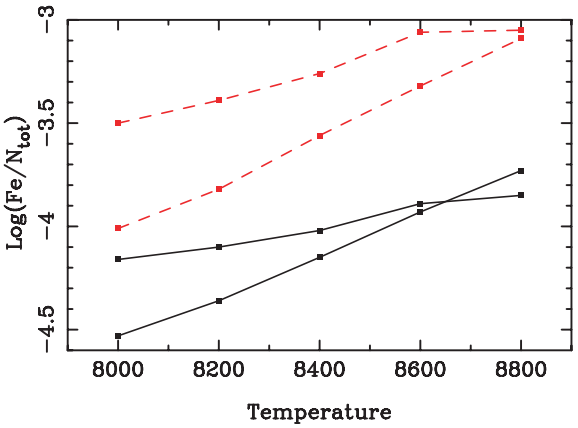

Figure 6. Ionization equilibrium: Fe I and II. The dashed lines are Fe I (upper) and Fe II (lower) using the standard stratification parameters. The lower lines are Fe I (mostly upper) and Fe II (mostly lower) without stratification. Values of $\log(\mathrm{Fe}/N_{\rm tot})$ refer to the deep photosphere [prior to the application of the function $g(x)$]. The four curves are based on lines with wavelengths longer than 3650 Å.

Stehlé–Hutcheon tables do not extend to large enough values of $N_{\rm e}$ for the higher Paschen lines.

At λ8750, P12, the lower gravity model provides a better fit to the wings than the $\log g = 4$ model, but the core is too deep. If we were to lower the observed continuum by 2–3 per cent, the overall fit, core and wings, is significantly better with the higher gravity model. Fig. 5 shows the Paschen line at λ8598, P14, which falls between the longer wavelength pair of the IRT. Again, the higher gravity model provides a better fit.

One may surely count Paschen lines to P18. It is arguable whether higher Paschen members are present. Thus the limiting Balmer and Paschen series are in agreement with one another, but a definitive interpretation awaits further study. Better observational material, specifically taken and reduced for the purpose of investigation of series confluence would also be useful.

The Paschen lines P13, P14, P15 and P16 are blended with present special problems because they are near the series confluence. Details are explained in Appendix A.

5 IONIZATION EQUILIBRIUM

Lines of Fe I and Fe II were chosen from a compilation of oscillator strengths by Fuhr & Wiese (2006). We used our line identification list (see URL below) to exclude cases with obvious blends. We then calculated abundances for models with $\log g = 3$ and 4 for $T_{\rm eff}$ ranging from 8000 to 8800 K. Calculations for all of these cases were made with, and without stratification. The stratification assumed was based on an analytic formula

$$g(x) = b + (1-b)\left[\frac{1}{2}\sqrt{\pi/a} \pm \frac{1}{2}\mathrm{erf}\left(\sqrt{a|x+d|^2}\right)\right]. \qquad (1)$$

In any given layer, the abundance of an element is multiplied by this $g(x)$. Here, $x = \log(\tau_{5000})$, and the negative sign is taken for $x \leqslant -d$. This function is a smoothed step of height $1 - b$, with the centre of the jump located at depth $\log \tau_{5000} = -d$. At large depths, $g(x)$ is nearly unity, while for the smallest depths, it has the value b. The Gaussian 1/e width of the step is $1/\sqrt{a}$.

For all spectra *other than those of Ca* II *and Sr* II, 'standard parameters' were used: $a = 6.7$, $\log b = -4$ and $d = 1$. We cannot claim any special validity for these particular values; they were used in CHCGW to reconcile profiles of the Ca K line and one line of the IRT. We have already explored a wide domain of parameter space, and must leave possible adjustments of the stratification parameters to account for anomalous ionization and excitation to future work.

Tables of wavelengths and equivalent widths may be found on our web page http://www.astro.lsa.umich.edu/cowley/hr710. For iron, abundances were found for five temperatures and two gravities, above and below the Balmer jump, and with and without stratification using the standard parameters. We made plots of abundances versus equivalent widths and excitation potential, and used the former plots to fix the microturbulent parameter. Trends for iron were removed by the value $\xi_{\rm t} = 3.5$. This value is somewhat large, but it also must account for the Zeeman broadening, which was not large enough to yield resolved patterns.

The results are illustrated in Fig. 6. Here, and elsewhere in this paper, '$\mathrm{N}_{\rm tot}$' means the sum of relative abundances of all elements. If $\log(H) = 12$, then $N_{\rm tot} = 1.03 \times 10^{12}$. We used 70 lines of Fe I and 32 lines of Fe II, all with wavelengths longer than 3650 Å. This plot is the primary basis for consideration of low-gravity (or low-pressure) models.

For the 8600 K, $\log g = 3$ model, with no stratification, we find

$$\log(\mathrm{Fe}/N_{\rm tot}) = -3.93\ (\mathrm{Fe\,I});\ \log(\mathrm{Fe}/N_{\rm tot}) = -3.89\ (\mathrm{Fe\,II}).$$

For iron, we made separate abundance determinations for lines below the Balmer jump. For 43 Fe I lines, we obtained $\log(\mathrm{Fe}/N_{\rm tot}) = -3.86$. This is less than 0.1 dex different from the value found for lines above the Balmer jump. Only eight lines of Fe II were found usable below the Balmer jump. These yielded $\log(\mathrm{Fe}/N_{\rm tot}) = -4.02$. In view of the smaller number of lines, we do not consider this value significantly different from the others. All calculations of iron below the Balmer jump were made without assuming stratification. We see no compelling evidence for stratification in iron.

The next richest spectra to Fe I and Fe II belong to Cr I and Cr II. We analysed 36 Cr I lines and 47 Cr II lines. Oscillator strengths were taken from VALD (see Kupka et al. 1999), but we omitted lines from intersystem transitions, where the multiplicity of the upper and lower terms are different. Experience has shown that *ab initio* and semi-empirical calculations for transitions permitted by Russell–Saunders coupling rules are somewhat more reliable than those for intersystem lines. Reasonable agreement was found for abundances from the Cr I and Cr II lines with wavelengths longer than 3650 Å,

from the 8600 K, $\log g = 3$ model, with no stratification:

$\log (\mathrm{Cr}/N_{\mathrm{tot}}) = -4.00$ (Cr I); $\log (\mathrm{Cr}/N_{\mathrm{tot}}) = -4.14$ (Cr II).

Several other elements are observed in two stages of ionization, but our results from them were less concordant. In particular, the spectra of Ti I and Ti II may be brought into better agreement by adjusting model parameters *or introducing stratification*. Details are tedious, and are omitted, pending a later investigation.

6 CALCIUM

6.1 The weaker Ca I and Ca II lines

We measured equivalent widths of 23 lines of Ca I, all with wavelengths longer than the Balmer jump. The equivalent widths spread evenly between 10 and 112 mÅ. With the 8600 K, $\log g = 3$ model, we obtained a mean $\log(\mathrm{Ca}/N_{\mathrm{tot}})$ of -4.65 ± 0.08 ($\xi_{\mathrm{t}} = 3.5$). There is no significant trend of the abundance with either equivalent width or excitation potential; the latter span a narrow range of 1.88–2.93 eV.

The Ca I resonance line, λ4227 was not included in the above average. It is only moderately strong ($W_{\lambda} = 169$ mÅ), and its core is in not at all unusual, like those of the K line or λλ4077 or 4215 of Sr II. We can fit the profile with $\log(\mathrm{Ca}/N_{\mathrm{tot}})$ of −4.65, and lowering the ξ_{t} to 1.5 km s^{-1}. We conclude λ4227 is in reasonable agreement with the weaker Ca I lines.

We found only seven useful Ca II lines, exclusive of H and K, and the IRT. The mean value of $\log(\mathrm{Ca}/N_{\mathrm{tot}})$ from all seven lines was -4.99 ± 0.33, with the 8600 K, $\log g = 3$ model. With these lines there were systematic trends both with excitation potential and equivalent width. Four lines, with excitation potentials averaging 7.2 eV gave $\log(\mathrm{Ca}/N_{\mathrm{tot}}) = -5.5$, while three lines with average χ_{ex} of 9.0 eV gave $\log(\mathrm{Ca}/N_{\mathrm{tot}}) = -4.2$. The tendency of high-excitation lines to give anomalously high abundance is a characteristic of the newly discussed anomalies of CP stars (cf. Ryabchikova et al. 2004). However, the abundance averages from Ca I and II are within the standard errors; we have not attempted to deal with the systematic trends.

One Ca II line is below the Balmer jump: 3461.87 ($\chi = 7.51$). The abundance from this single line is $\log(\mathrm{Ca}/N_{\mathrm{tot}}) = -4.6$. We make no judgement about stratification from this single line.

6.2 The K line

The Ca II K line exhibits the full symptoms of stratification. An attempt to fit it with the abundance obtained from the Ca I or Ca II lines (cf. above) results in a deep, broad core, as shown in Fig. 7. The plot is quite similar to fig. 3 of Ryabchikova et al. (2002) for the star γ Equ. Here, and in similar figures to follow, only token efforts were made to fit the atomic line spectrum apart from the feature of direct interest.

The stratification parameters given in the caption to Fig. 7 were determined by trial and error. They imply an abundance jump of seven orders of magnitude between optical depths $\log(\tau_{5000}) = -0.7$ and +0.3.

6.3 The IRT

Lines of the IRT manifest stratification in a way that is somewhat similar to the Ca II K line, though the total absorption is much less, and the central absorption is more significant relative to the total profile. We must keep in mind that the possible influence of surficial

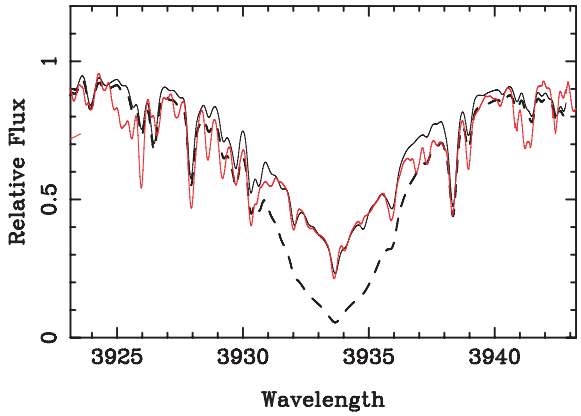

Figure 7. The Ca II K line, observed (solid grey) and calculated with stratification. The stratification parameters for $g(x)$ are: $a = 6.7$, $\log b = -7.0$, $d = 0.25$ and $\log(\mathrm{Ca}/N_{\mathrm{tot}}) = -3.10$. The heavy dashed line is for $\log(\mathrm{Ca}/N_{\mathrm{tot}}) = -4.65$, and *no* stratification.

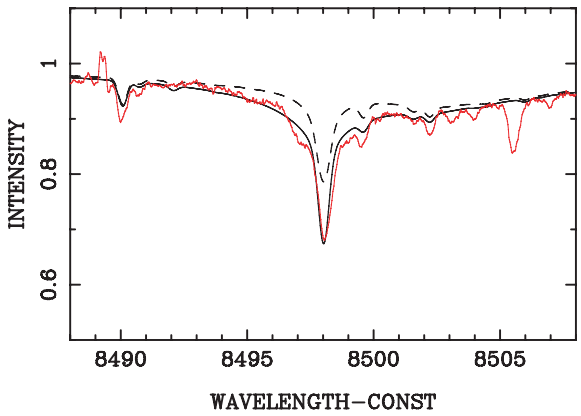

Figure 8. The Ca II λ8498 line, observed (solid grey) and calculated (solid black) with stratification. The stratification parameters for $g(x)$ are: $a = 6.7$, $\log b = -5.70$, $d = 0.25$. $\log(\mathrm{Ca}/N_{\mathrm{tot}}) = -2.12$. The dashed line is for the parameters used to fit the Ca II K line (see Fig. 7). Both calculations employed a model with $\log g = 4$.

abundance patches which could have an influence on the profiles of the IRT. In view of the better fits with $\log g = 4$ for P14, which falls between λ8498 and λ8542 of the IRT, as well as lower Paschen all calculations illustrated for the IRT have used the higher gravity.

Fig 8 shows observed and computed profiles for λ8498 in HR 710. Damping wings are present, but the stellar profiles change rapidly in structure, from core to wing. These shapes can arise if the abundance of calcium varies with a stratification function $g(x)$ as described above.

Note the extraordinarily high value of calcium required for the deep photosphere, and the large abundance gradient implied by the parameters of the function $g(x)$.

The fit to the strongest line of the IRT, λ8542, is shown in Fig. 9. The wings of this line are significantly stronger than those of the weaker λ8498 line. The best fit (solid line) used different stratification parameters from those used to fit the weaker λ8498 line (dashed line), though the abundance in the deep photosphere is roughly similar: $\log(\mathrm{Ca}/N_{\mathrm{tot}}) = -2.5$ versus −2.1. Several lines of neutral calcium are in the region of Fig. 9. Two of the lines, at 8525.72 and 8555.51, were strong enough to require explicit inclusion in the calculation. The scaling factor $g(x)$ had to be applied to them, as

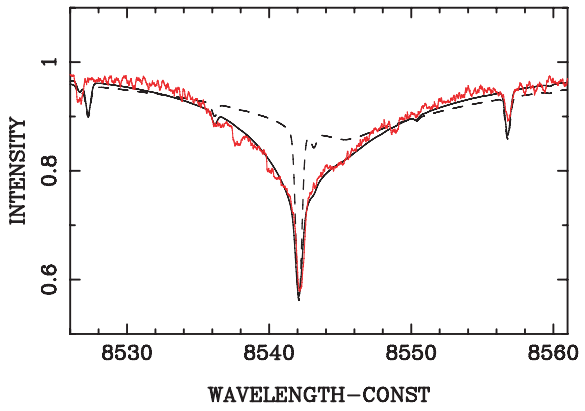

Figure 9. The Ca II λ8542 line, observed (solid grey) and calculated (solid black) with stratification. The stratification parameters for $g(x)$ are: $a = 1.0$, $\log b = -6.70$, $d = -1.0$. $\log(\mathrm{Ca}/N_{\mathrm{tot}} = -1.52$. The function $g(x)$ differs from unity throughout the atmosphere, so the effective $\log(\mathrm{Ca}/N_{\mathrm{tot}})$ at $\log(\tau_{5000}) = 0.0$ is roughly −2.52, in fair agreement with the value necessary to fit the λ8498 line. The dashed line is for the parameters used to fit the λ8498 line. Both calculations use $\log g = 4$.

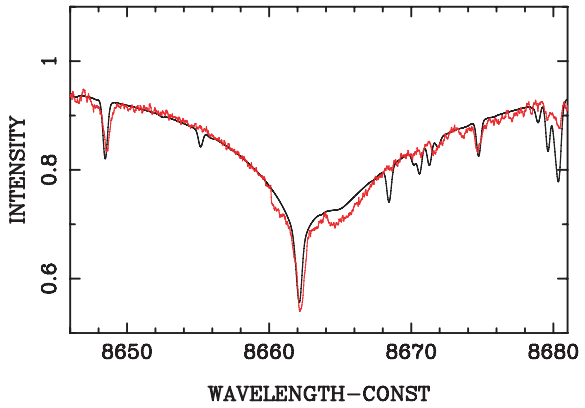

Figure 10. The Ca II λ8662 line, observed (solid grey) and calculated (solid black) with stratification. The calcium abundance and stratification parameters are *identical* to those used to fit the λ8542 line. The model has $\log g = 4$.

well as λ8542. Otherwise, with the $\mathrm{Ca}/N_{\mathrm{tot}}$ assumed for the deep photosphere, they would have been huge.

Fig. 10 shows the third member of the IRT, λ8662. No adjustment of the parameters from those used to fit the λ8542 line has been made.

7 STRONTIUM

7.1 Weaker subordinate lines

In addition to the resonance lines λλ4077 and 4215, and the stronger subordinate lines λλ4161 and 4305, we found five marginally unblended lines of Sr I and Sr II, and determined provisional abundances from them. Results are shown in Table 1 for the 8600 K, $\log(g) = 3$ model. The abundances are up to a factor of 3 lower if the $\log(g) = 4$ model is used, but the agreement between the first and second spectra is still within 0.1 dex for the lower microturbulence. The weaker, Sr I lines, which are less sensitive to microturbulence, magnetic broadening and surface gravity give mean abundances of −6.3 and −6.4 for the lower and higher values of ξ_{t}, respectively.

Table 1. Abundances from weaker subordinate Sr lines: 8600 K, $\log(g) = 3$.

Spectrum	λ (Å)	W_λ (mÅ)	$\log(\mathrm{Sr}/N_{\mathrm{tot}})$	
			$\xi_{\mathrm{t}} = 1.3$	$\xi_{\mathrm{t}} = 3.5$
Sr II	3380.69	97	−6.39	−7.70
Sr II	3474.89	83	−5.96	−7.23
Sr I	6408.44	23	−6.21	−6.31
Sr I	6504.00	20	−6.07	−6.15
Sr I	6617.27	18	−5.87	−5.93
Averages			−6.10	−6.66
$\log(\mathrm{Sr}/\mathrm{Sr}_\odot)$			+3.02	+2.96

We have not experimented extensively with stratification. The parameters used to get a fit for λ4077 (see below) give unacceptably high abundances from the weak Sr I lines. The 'standard' stratification parameters, $a = 6.7$, $\log b = -4.0$ and $d = +1$, reduces the abundance difference between the first and second spectra though only by a little, and the overall abundances increase by more than a dex.

We conclude that a reasonable mean abundance for the atmosphere of HR 710 is $\log(\mathrm{Sr}/N_{\mathrm{tot}}) \approx -6.4$. This is a factor of 2.5 higher than the abundance found by Ryabchikova et al. (1997) for the strontium star γ Equ. It comports well with our assertion, based on Fig. 1, that strontium is somewhat stronger in HR 710 than γ Equ.

7.2 The resonance lines

We were unable to fit the near wings of the stronger resonance line, λ4077, without moving the abundance jump deep into the photosphere. The adopted parameters given in Fig. 11 lead to $g(x) = 0.770$ at the deepest layer of our atmosphere, $\log(\tau_{5000}) = 1.4$. The strontium fraction decreases rapidly from the deepest layers, and levels to the value $b\,(\mathrm{Sr}/N_{\mathrm{tot}}) = 2 \times 10^{-11}$ by $\log(\tau_{5000}) = -5.4$

Fig. 12 shows the abundance stratification profiles of strontium and calcium.

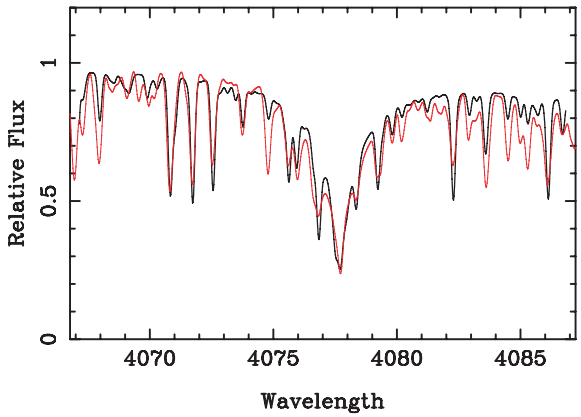

Figure 11. The Sr II λ4077 line, observed (solid grey) and calculated (solid black) with stratification. The parameters of the fit are: $a = 1.7$, $\log b = -6.70$, $d = -1$, $\log(\mathrm{Sr}/N_{\mathrm{tot}}) = -4.00$. At $\log(\tau_{5000}) = 0.0$, $\log(\mathrm{Sr}/N_{\mathrm{tot}}) = -4.85$. This is still considerably larger than the value obtained from the weak lines (Table 1): −6.10, with $\xi_{\mathrm{t}} = 1.3$.

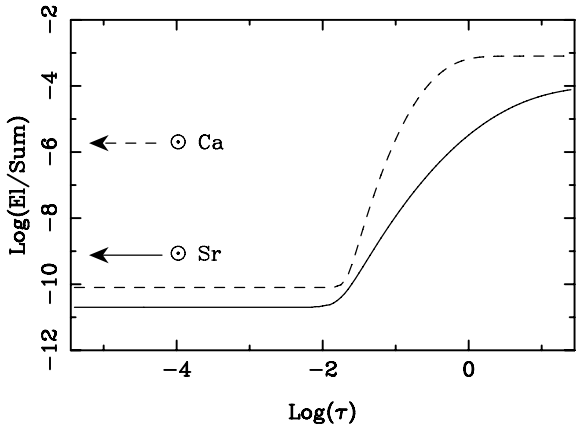

Figure 12. Stratified abundances of strontium (solid) and calcium (dashed) using parameters appropriate for the λ4077 and K line, respectively. Solar abundances are indicated.

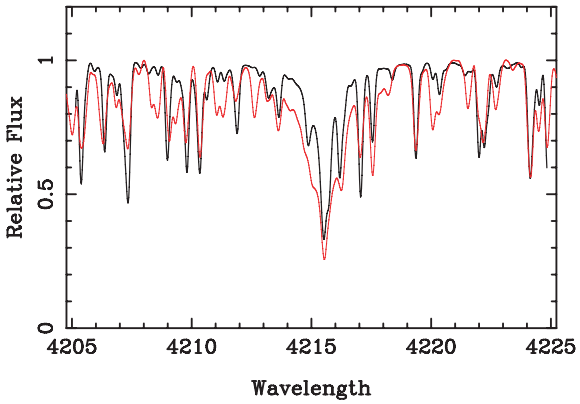

Figure 13. The Sr II λ4215 line, observed (solid grey) and calculated (solid black) with stratification. The parameters *are the same* as those used in the fit for λ4077. A considerably better fit (not shown) can be obtained from a slight modification of the parameters to: $a = 1.7$, $\log b = -6.70$, $d = -1$, $\log(\mathrm{Sr}/N_{\mathrm{tot}}) = -3.70$.

The weaker of the resonance lines, λ4215, is shown in Fig. 13. The calculation shows used the same fitting parameters as those used for the stronger line. It is unclear just how meaningful this might be, since the blending is quite significant, and extends well into the core of the profile.

7.3 The subordinate Sr II lines

Fig. 14 shows a calculation of the subordinate line, λ4161.80, $5p^2P^0_{1/2}$–$6s^2S_{1/2}$. The line is in Sr II multiplet 3. Only the long-wavelength part of the profile is sufficiently unblended for use in fixing the stratification parameters. The calculation shows the result of using the parameters from the best λ4215 fit, which is poor. While we were able to improve the fit in the red wing somewhat, by trial-and-error adjusting the parameters of $g(x)$, we never achieved a satisfactory fit. When the near wing, marked 'W' in the figure, was fitted, the calculated continuum (C) was below the observed one.

A similar situation was found for the stronger line of multiplet 3, λ4305, though for this line it was the violet wing that proved most useful (cf. Fig. 1).

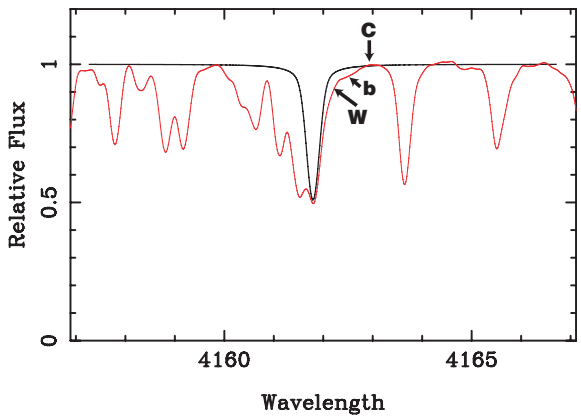

Figure 14. The Sr II λ4162 line, observed (solid grey) and calculated (solid black) with stratification. The parameters of the fit are: $a = 1.7$, $\log b = -7.0$, $d = -1$, $\log(\mathrm{Sr}/N_{\mathrm{tot}}) = -3.70$, the same as for the λ4077 resonance line. Other atomic lines have been omitted in the calculated profile for clarity. The near wing (W) and continuum (C) are noted. The observed violet wing contains a weak absorption, primarily due to Fe I (b). It is not strong enough to confuse the location of the near wing of the Sr II line.

Table 2. Summary of stratification parameters.

λ (Å)	log(El/N$_{\mathrm{tot}}$)	a	log b	d	Remarks
		Ca II			
3933	−3.10	6.7	−7.00	0.25	Fig. 7
3933	−4.00	6.7	−6.00	0.50	log g = 4
8498	−2.12	6.7	−5.70	0.25	Fig. 8
8542	−1.52	1.0	−6.70	−1.0	Fig. 9
8662	−1.52	1.0	−6.70	−1.0	Fig. 10
		Sr II			
4077	−4.00	1.7	−6.70	−1.0	Fig. 11
4215	−3.70	1.2	−6.70	−1.0	See text
4162	−3.70	1.7	−7.00	−1.0	Fig. 14

In all likelihood, a satisfactory fit could be found with a more elaborate stratification model than the one fixed by the parameters of our $g(x)$ function. We do not explore this here.

8 STRATIFICATION AND HR 710

8.1 Summary of stratification parameters

Stratification parameters are collected in Table 2. The second entries for λ3933 give a good fit to the core and wings (to ca. ±40 Å) for a surface gravity $\log g = 4.0$. There is no corresponding figure. The entries for Sr II λ4215 are the values mentioned in the caption to Fig. 13, which give an improved fit. Note that (El/N_{tot}) refers to the deepest photospheric layers.

8.2 General remarks

The near wings and cores of strong lines in magnetic CP stars cannot be fitted with traditional models. Non-LTE is surely relevant, but it is most unlikely to account for all of the discrepancies between theory and observation. Modern workers have returned to the notion of 'anomalous atmospheres, or AA', a term coined by Underhill (1966). Kochukhov, Bagnulo & Barklem (2002) showed that the

Balmer-line profiles could be fitted with an ad hoc modification of the temperature distribution in the high photosphere. Ryabchikova and colleagues (cf. Ryabchikova 2005) have used stratified abundance models to explain both the cores and near wings of strong lines of Ca II *and* anomalous excitation and ionization, often seen in magnetic CP stars.

One might expect that the same stratification model would fit all of the Ca II lines, H and K, and the IRT. This was not the case for HR 710. We must note that our stratification model is somewhat more constrained, by Equ. 1, than those used by Ryabchikova and coworkers.

The cores of the resonance lines of Sr II, λλ4077 and 4215 exhibit similar peculiarities to the K line. Vastly improved fits can be obtained using stratified models, though slightly different stratifications are required. The subordinate lines, λλ4162 and 4305 require stratification or other modifications to fit the wings. The stratification parameters required to fit λ4077, however, make very little difference in the wings of the two subordinate lines.

Ionization and excitation anomalies are present in the HR 710 spectrum. The Ti I and II ionization and excitation imbalance deserves further study. The rich Fe I and Fe II spectra were in satisfactory agreement without the need for stratification, provided we employed the significantly low-gravity model with $\log g = 3.0$.

Generally, the line spectrum in the red and infrared was fitted better by a higher gravity model, and the relevant illustrations shown are based on that model. We cannot rule out the relevance of abundance patches for our difficulties in fitting all of the Ca II or the Sr II lines with a single stratification model.

9 HR 710AA AND ITS COMPANION HR 710AB

The mass function for an SB1 system is $f(m) = m^3 \sin^3(i)/(m + M)^2\,\mathrm{M}_\odot$, where M and m are the masses of the primary and secondary, respectively. This $f(m)$ was well determined by Bonsack, and has the value 1.777×10^{-3}.

For a given m and $f(m)$, the orbital inclinations decrease as $M \rightarrow m$. Kitamura (1980) noted that the inclinations of short-period Ap SB1 stars tend to be small. Such near pole-on views of SB1 systems would require a subluminous star, since the companion spectrum is unseen. Bonsack suggested a white dwarf for HR 710. This model explains the failure of the magnetic field to show an obvious reversal.

If we assume the 3-d orbital period is also the period of rotation of the primary, the observed $v \sin i$ depends directly on the radius of the star and the inclination of its rotational axis.

The equatorial velocity of a star is

$$v_{\mathrm{eq}} = \frac{50.56R}{P}, \qquad (2)$$

where R is in solar radii and P in days.

Values of $v \sin i$ have been published by Bonsack (1981) and Preston (1971): 7.7 and 13 $\mathrm{km\,s^{-1}}$, respectively. We have made a new determination from our UVES spectra, using the magnetic null lines λλ3850, 4006, 4065 and 7090, all of Fe I.

The observations were (Fourier) unfiltered, but they were interpolated to every 0.02 Å, for compatibility with MICHIGAN software. We assumed a Gaussian 1/e width of 0.04 Å for the instrumental profile in the blue–violet. This allows for a small degradation of the resolution; a resolving power, $\mathcal{R}$ of 80 000 would give ca. 0.03 Å for the 1/e width, where we use $\Delta\lambda = \lambda/\mathcal{R}$ as the full width at half-maximum of the instrumental profile. For λ7090, using $\mathcal{R} = 110\,000$, the 1/e width of the pure instrumental profile is 0.045 Å, and we assumed 0.055 Å.

Table 3. Secondary mass m for various primary masses M and $v \sin i$. The preferred values are in bold face.

$M/\mathrm{M}_\odot$	$R/\mathrm{R}_\odot$	i (°)	$v \sin i$		
			8	**10**	12
2.00	1.74	29	0.89	0.68	0.56
1.84	**1.63**	28	0.79	**0.62**	0.48
1.60	1.46	25	0.64	0.49	0.40

Synthetic spectra were fitted to regions containing these lines spectra, and the best fits determined by trial and error. We find that a value of 10 $\mathrm{km\,s^{-1}}$ gives the best overall fit. This is near the mean of the Preston and Bonsack's published values. However, because of blending, and subjective judgements about a fit, the uncertainty of $v \sin i$ is still between 1 and 2 $\mathrm{km\,s^{-1}}$.

We prefer $M/\mathrm{M}_\odot = 1.84$ and $R/\mathrm{R}_\odot = 1.63$ from tables in Drilling & Landolt (1999), for a main-sequence A-star with an effective temperature of 8600 K. The values agree well with Hubrig et al. (2007).

It is now straightforward to get the inclination from equation (2), if we assume a 3-d period. From the inclination, the secondary mass, m, will follow from the mass function, given a primary mass, M. In order to provide some indication of the overall uncertainties, we give the secondary mass in Table 3, for three assumed masses (and corresponding radii), and three values of $v \sin i$. We assume the relation between mass and radius for main-sequence stars given by Drilling & Landolt (1999).

Our preferred values give $m = 0.62\ \mathrm{M}_\odot$, conveniently near the most probable observational value for white dwarf masses according to Weidemann (1990). This supports the assertion of Czesla & Schmitt (2007) that the secondary of HR 710Aa 'is clearly a very plausible candidate for the observed X-ray emission ...'. These authors discuss a magnetically confined wind-shock model.

Bonsack (1981) also discussed a 15.88-d magnetic period. With $R = 1.63\,\mathrm{R}_\odot$, this period leads to an equatorial velocity of 5.2 $\mathrm{km\,s^{-1}}$, incompatible with the adopted $v \sin i$. To reconcile this period with the observed $v \sin i$, we would need to assume a stellar radius nearly double that used. This is not compatible with the luminosity of the star.

10 REMARKS AND CAVEATS

The present work on HR 710 shows that it is difficult to explain the profiles of strong Ca II and Sr II lines with a simple abundance-stratified model. Overall, we strongly support the stratification models, but find indications that refinements are necessary.

Different stratification parameters were required for the K line and the IRT of Ca II, while Sr II lines also required adjustments of the parameters for individual lines.

It remains to be seen whether theoretical work can explain the large elemental abundances of the best-fitting stratification models. These require very high abundances in the deep photosphere in order to explain the observed, broad wings. In the case of calcium, traditional diffusion calculations have explained low photospheric abundances (Am stars).

Among a number of uncertainties in the present discussion, we note that our stratification model $[g(x)]$ (i) may not have explored the optimum domains of parameter space or (b) may have been too simplistic. Regarding the latter point, we note the sophisticated approach of Kochukhov et al. (2006).

Eventually, it will prove necessary to approach the modelling of the spectra of these stars with improved methods. Useful modifications of our procedures might include changing the $T - \tau$ relation in the high photosphere. This has already been shown to give fits to the Balmer lines (Kochukhov et al. 2002), and can give nibs on the K line (Cowley, Hubrig & Kamp 2006). In the last reference, it was also pointed out that sharp K line nibs could result if the gas pressure in the upper atmosphere were lowered.

Calculations done in LTE must be considered provisional until supported by work done with non-LTE. This is especially true for the upper atmospheres, where the total radiative flux is very nearly constant, independent of local conditions. The core of the Ca K line is formed highest of lines considered in this work, and Cowley, Hubrig & Kamp showed that LTE calculations were only slightly modified by non-LTE.

The greatest challenge of the observations of strong-line profiles of CP stars is to the theoretician. It is straightforward to make ad hoc adjustments to a model until a profile is fitted. It is quite another to justify such modifications with rigorous calculations.

ACKNOWLEDGMENTS

We thank Dr Paul Barklem for permission to use his code WCALC for calculation occupation probabilities of hydrogen levels, and Dr Pierre North, for pointing out the short-period system HD 200405. CRC is grateful for past use of the facilities of the Dominion Astrophysical Observatory. He also thanks colleagues at Michigan and elsewhere for helpful comments. We thank the referee, Lars Freyhammer, for many valuable comments, corrections and suggestions. This research has made use of the SIMBAD data base, operated at CDS, Strasbourg, France.

REFERENCES

Babcock H. W., 1958, ApJS, 3, 141
Barklem P., 2004, http://www.astro.uu.se/∼barklem/, see hbop.f
Bonsack W. K., 1981, PASP, 93, 756
Carrier F., North P., Udry S., Babel J., 2002, A&A, 151, 169
Castelli F., Hubrig S., 2004, A&A, 421, L1
Cowley C. R., 1970, The Theory of Stellar Spectra. Gordon & Breach Science Publishers, London, p. 213
Cowley C. R., 2000, Observatory, 120, 318
Cowley C. R., Hubrig S., Ryabchikova T. A., Mathys G., Piskunov N., Mittermayer P., 2001, A&A, 367, 939
Cowley C. R., Hubrig S., Kamp I., 2006, ApJS, 163, 393
Cowley C. R., Hubrig S., Castelli F., González J. F., Wolff B., 2007, MNRAS, 377, 1579 (CHCGW)
Cunto W., Mendoza C., Ochsenbein F., Zeippen C. J., 1993, A&A, 275, L5
Czesla S., Schmitt J. H. H. M., 2007, A&A, 465, 493
Drilling J. S., Landolt A. U., 1999, in Cox A. N., ed., Allen's Astrophysical Quantities, 4th edn. Springer-Verlag/Am. Inst. Phys., New York, p. 381
Fletcher J. M., Harmer C. F. W., Harmer D. L., 1980, Publ. Dom. Astrophys. Obs. Victoria BC, 15, 405
Fuhr J. R., Wiese W. L., 2006, J. Phys. Chem. Ref. Data, 35, 669
Hubrig S., North P., Schöller M., 2007, Astron. Nachr., 328, 475
Hünsch M., Schmitt J. H. M. M., Voges W., 1998, A&AS, 132, 155
Kaiser A., 2006, in Sterken C., Aerts C., eds, ASP Conf. Ser. Vol. 349, Astrophysics of Variable Stars. Astron. Soc. Pac., San Francisco, p. 257
King J. R., Villareal A. R., Soderblom D. R., Gulliver A. F., Adelman S. J., 2003, AJ, 125, 1980
Kitamura M., 1980, Ap&SS, 68, 283
Kochukhov O., Bagnulo S., Barklem P. S., 2002, ApJ, 578, L75
Kochukhov O., Tsymbal V., Ryabchikova T., Makaganyk V., Bagnulo S., 2006, A&A, 460, 831
Kupka F., Piskunov N. E., Ryabchikova T. A., Stempels H. C., Weiss W. W., 1999, A&AS, 138, 119
Künzli M., North P., Kuruca R. L., Nicolet B., 1997, A&AS, 122, 51
Lemke M., 1997, A&AS, 122, 285
Moore C. E., 1945, Cont. Princeton Univ. Obs., No. 20
Preston G. W., 1971, ApJ, 164, 309
Roman N. G., 1949, ApJ, 110, 205
Ryabchikova T., 2005, in Alecian G., Richard O., Vauclair S., eds, EAS Publ. Ser. Vol. 17, Element Stratification in Stars: 40 Years of Atomic Diffusion. EAS, Les Ulis, p. 253
Ryabchikova T., Adelman S. J., Weiss W. W., Kuschnig R., 1997, A&A, 322, 234
Ryabchikova T., Piskunov N., Kochukhov O., Tsymbal V., Mittermayer P., Weiss W. W., 2002, A&A, 384, 545
Ryabchikova T., Nesvacil N., Weiss W. W., Kochukhov O., Stütz C., 2004, A&A, 423, 705
Ryabchikova T., Kochukhov O., Bagnulo S., 2007, in Romanyuk I. I., Kudryavtsev D. O., eds, Proc. Int. Conf., Physics of Magnetic Stars, preprint (astro-ph/0703296)
Searle L., Lungershausen W. T., Sargent W. L. W., 1966, ApJ, 145, 141
Stehlé C., Hutcheon R., 1999, A&AS, 140, 93
Sugiura M. Y., 1927, J. Phys. Radium, 8, 113
Tokovinin A. A., 1997, A&AS, 121, 71
Underhill A., 1966, in Hubenet H., ed., IAU Symp. 26, Abundance Determinations in Stellar Spectra. Academic Press, London
Vidal C. R., Cooper J., Smith E. W., 1973, ApJS, 25, 37
Weidemann Y., 1990, ARA&A, 28, 139

APPENDIX A: CALCULATION OF HIGHER PASCHEN LINES

Calculations near series limits need to account for overlapping lines, as well as the 'dissolution' of some discrete upper levels by various perturbations from the plasma bath of the emitting and absorbing atoms. We have implemented the scheme outlined in Cowley (2000) in conjunction with a probability function $W(n)$ for the existence of discrete upper levels. The specific routine was from Barklem (2004). The basic assumption is that we can calculate the total opacity due to both bound–bound and quasi-continuous absorption by considering only a wavelength region near a given bound–bound transition. These regions extend from the halfway points between transitions to level $n - 1$ and n, and from n to $n + 1$. We shall refer to these regions as the *n-local regions*. Following the reference cited, we define an n-dependent cross-section, such that for a Paschen line

$$\int \sigma_{3n} \mathrm{d}\Delta\lambda = \frac{\pi e^2}{mc^2} \lambda_n^2 f_{3n}.$$

The integral here is assumed to extend *only* over the n-local region. The cross-sections so defined are in excellent agreement with those found in TOPbase (Cunto et al. 1993) for photon energies below the ionization limit.

Line absorption in the n-local region is calculated in the usual way, but with the product $N_3 f_{3n}$ diminished by the occupation probability $W(n)$. However, the line profile is truncated at each end of the n-local region. The ordinary continuous opacity is then augmented by an amount necessary to bring the total absorption into agreement with the above equation. In this way the total absorption merges smoothly with the known photoelectron absorption cross-section at the series limit, as has been known for many years (Sugiura 1927).

This paper has been typeset from a TEX/LATEX file prepared by the author.